AUT Journal of Mechanical Engineering

AUT J. Mech. Eng., 2(1) (2018) 39-50
DOI: 10.22060/mej.2017.12960.5486

Energy and Exergy Analysis and Optimization of a Heat Sink Collector Equipped with Rotational Obstacles

S. Sadripour[1, 2], A. A. Abbasian Arani[1] , S. Kermani[1]

[1] Department of Mechanical Engineering, University of Kashan, Kashan, Iran
[2] Faculty of Mechanical Engineering, University of Shahreza, Shahreza, Iran

ABSTRACT: In this paper, the forced convection flow in a heat sink collector equipped with stationary and rotational obstacles is studied numerically. Three-dimensional governing equations are solved by control volume approach based on the SIMPLE algorithm and k–ε turbulence model. Reynolds numbers are considered in the laminar-turbulent range of 50 < Re < 12,000. The optimization was carried out by variation of related parameters. It is concluded that using heat sink, instead of a customary instrument, increases the outlet temperature from the collector and exergy efficiency due to longer installing of the fluid inside the collector. Also, it is realized that using the stationary and rotational obstacles enhance the outlet fluid temperature (about 2.5°C), energy efficiency and exergy efficiency. Nevertheless, using the rotational obstacles is more effective than the stationary obstacles. While the trend of exergy efficiency variation with effective parameters is increasing, applying the obstacles precipitates the efficiency increment (from 4% to 5.3%). In addition, for the case that the trend of exergy efficiency variation by changing these parameters is decreasing, the decreasing trend gets slow. There is a unique mass flow rate (0.005 kg/s) that the exergy efficiency gets a maximum value and for the higher mass flow rates, the efficiency decreases slightly and then remains unchanged.

Review History:

Received: 4 June 2017
Revised: 25 October 2017
Accepted: 30 October 2017
Available Online: 5 December 2017

Keywords:

Heat sink collector
Rotational obstacles
Exergy optimization
Forced convection
Radiation

1- Introduction

The sun is the source of life on the earth, but at the same time, it is a free source of energy for many systems using this resource for doing a process. The greatest advantage of solar energy as compared with other sources of energy is that it is clean and can be supplied without any environmental pollution [1-4]. Furthermore, solar energy has a remarkably higher potential compared to other renewables energy, such as wind, ocean, hydro, biomass and geothermal. There are many types of systems that employ solar energy collectors as a source of input energy to drive a process. Between these systems, the flat-plate solar collector has a simple design and low costs of construction compared with other collector types. In addition to the direct solar radiation absorption, they can also absorb the diffuse radiation [5]. So far a lot of numerical and empirical studies related to solar collectors have been conducted. The results of these studies demonstrate that the overall performance of collector is related to many factors, including the distance between absorber plate and glass cover, pipe diameter [6, 7], wind velocity [8], solar radiation [9], collector material [10], flow rate [11], and channel depth [12]. One proper technique to improve the solar collector's efficiency is to use the heat sink below the absorber plate instead of pipes. It can increase the wetted surface between fluid and absorber, and also increase the outlet temperature of the fluid. Furthermore, employing obstacles in the heat exchangers has been one of the frequent approaches to break the laminar sub-layer and create local turbulence due to flow separation and reattachment between successive obstacles, which reduces the thermal resistance and significantly enhances the heat transfer [13]. This paper focuses on the energy analysis of heat sink flat plate solar collector equipped with obstacles to enhance the thermal performance and achieve the maximum energy efficiency and exergy efficiency under given operating conditions.

Baniamerianand et al. [14] studied numerically aerodynamic coefficients of solar troughs considering terrain effects and vortex shedding. Their results showed that in order to properly align trough collector in solar farms, it is essential to study the created vortices shed at the behind of parabolic troughs. In another numerical study, Ziapour and Rahimi [15] investigated a natural convection heat transfer in a horizontal wavy absorber solar collector using the second law analysis. Their results showed that by increasing the cosine wave amplitude, the collector irreversibility decreases. Ajay and Kundan [16] studied the performance evaluation of parabolic solar collector filled with nanofluid ($Al_2O_3/H_2O–C_2H_6O_2$) using both experimental and CFD techniques. Their results showed a close agreement between experimental and CFD result.

A method for establishing the optimal operation mode of solar collectors can be derived from the exergy analysis of the processes specific for the fluid that passes through the collector's stream tube [17]. The analyzed relevant literature contains studies on the dependence of the exergy efficiency on the fluid flow rate and fluid temperature at the entrance into the collector serpentine pipe. Based on results of the referred reference, the specific exergy of the fluid in the solar collector as depending on the inlet temperature, the parameter being either the solar radiation or the fluid flow rate, can present points of local maximal. These aspects are not highlighted in the energy efficiency equation. Shojaeizadeh and Veysi

Corresponding author, E–mail: abbasian@kashanu.ac.ir

[18] developed a correlation for parameter controlling exergy efficiency optimization of an Al_2O_3/water nanofluid based flat-plate solar collector. Said et al. [19] investigated energy and exergy analysis of a flat-plate solar collector using dispersed different diameter sizes of Aluminum oxide nanoparticles (of used nanofluid) and they founded that the combination of energy and exergy analysis is an appropriate method to optimize the flat-plate solar collectors.

As can be seen, in most of the aforesaid studies, stationary obstacles have been considered to improve the efficiency of heat sink flat-plate air heaters. But, based on above literature review, it can be observed that the effect of using rotational obstacles in water-based heat sink solar collectors has never been reported. Thus, the objective of this study is to investigate the energy and exergy analysis of a water-based flat-plate solar collector that is equipped with stationary and rotational obstacles numerically using finite volume method.

2- Methodology

2- 1- Physical model

The three-dimensional schematic diagram of the heat sink of a flat-plate solar collector equipped with obstacles is shown in Fig. 1. Table 1 represents different properties of this heat sink collector. The geometrical aspect of the presented collector is the same as the used collector in the reference [5]. The reason for this selection is the empirical data available for the following analysis. For simulation, the useful received energy by a collector is calculated based on inlet solar radiation and overall heat loss using analytical relations. In the following, the three-dimensional heat sink collector with and without obstacles simulated numerically and useful received energy by fluid, the outlet temperature of fluid and energy and exergy efficiencies were calculated. The flow inside the channel is considered at steady state condition and turbulent flow regime. The heat transfer and flow field are studied for the simple heat sink collector (with no obstacle) and also a collector equipped with stationary and rotational cylindrical insulated obstacles. Velocity inlet boundary condition with different mass flow rates as inlet boundary condition and pressure outlet as outlet boundary condition is assumed for the inlet section and the outlet section of the heat sink collector. The absorber plate is produced from Aluminum with matted black color. The referred collector is under the uniform heat flux that is calculated using optical properties

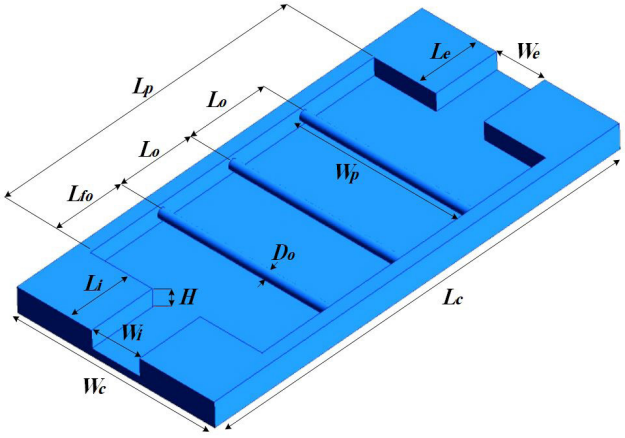

Fig. 1. Schematic diagram of the heat sink of a flat-plate solar collector equipped with obstacles

Table 1. Properties of heat sink collectors simulated in the present study

Properties	Symbol	Value
Dimensions of collector	$L_c \times W_c$,mm	200×92.5
Dimensions of the inlet section	$L_i \times W_i$,mm	10×20
Dimensions of the exit section	$L_e \times W_e$, mm	10×20
The height of heat sink	H, mm	1.5
Slop of collector	B	35°
Quantities of glass covers	N	1
The emissivity of glass covers	ε_g	0.85
Thickness of plate	δ_p, mm	0.1
Emissivity of plate	ε_p	0.9
The thermal conductivity of the plate	k_p ,W·m^{-1}·K^{-1}	211
Optical efficiency	η_0	0.68
Thickness of insulators	δ_i , mm	2.0
The thermal conductivity of insulators	k_i ,W·m^{-1}·K^{-1}	0.05
Quantities of obstacles	n_o	3
Location of the first obstacle	L_{fo} , mm	38
Location of another obstacle	L_o , mm	50
Diameter of obstacles	D_o, mm	0.5

and overall heat loss of collector for different sunny hours based on empirical measurements results of Khorasanizadeh et al. [5] for a reference collector in Tehran located in Iran (Table 2). In simulating of stationary obstacles and moving wall assumptions, no-slip boundary condition is considered. Also, all of these obstacles with a diameter of D_o are insulated. Because of considering influences of overall heat loss in calculating of useful received energy by the collector, other

Table 2. Empirical results of Khorasanizadeh et al. [5] for the reference collector installed in Tehran

Time	I_T ,W·m^{-2}	T_a ,°C	T_{in} ,°C	V_w , m·s^{-1}
09:00	560	33	44.5	6
09:30	630	33	45	6
10:00	750	34	46	5
10:30	830	35	47	6
11:00	925	36	50	6
11:30	992	37	51	5
12:00	1006	38	53	5
12:30	1020	38.5	54	6
13:00	978	40.5	56	6
13:30	914	40.5	57	5
14:00	834	41	60	5
14:30	780	41	61	4
15:00	734	39.5	62	5
15:30	626	41	63	6
16:00	607	41	64	6

walls of the heat sink are assumed insulated.

2- 2- Governing equations

The system of governing equations for fluid flow and heat transfer in the flat–plate solar collector can be written in the Cartesian tensor system as [20]:

$$\frac{\partial}{\partial x_i}(\rho u_i) = 0 \tag{1}$$

$$\frac{\partial}{\partial x_j}(\rho u_i u_j) = -\frac{\partial P}{\partial x_j} + \frac{\partial}{\partial x_j}\left[\mu\left(\frac{\partial u_i}{\partial x_j} + \frac{\partial u_j}{\partial x_i}\right)\right] + \frac{\partial}{\partial x_j}\left(-\rho\overline{u_i' u_j'}\right) \tag{2}$$

$$\frac{\partial}{\partial x_i}(\rho u_i T) = \frac{\partial}{\partial x_j}\left[\left(\frac{\mu}{\mathrm{Pr}} + \frac{\mu_t}{\mathrm{Pr}_t}\right)\frac{\partial T}{\partial x_j}\right] \tag{3}$$

where ρ is the fluid density and u_i is the axial velocity, μ, $\acute{u}$ and u_j are the fluid viscosity, fluctuated velocity and the axial velocity, respectively, and the term $\overline{\rho u_i' u_j'}$ is the turbulent shear stress.

By using the Reynolds averaged approach for modeling the flow field and heat transfer in turbulence flow regime, it is required to model the Reynolds stresses $\overline{\rho u_i' u_j'}$ in Eq. (2). For the closure of the equations, the k–ε turbulence model was chosen. A common method employs the Boussinesq hypothesis to relate the Reynolds stresses to the mean velocity gradient as [20]:

$$-\rho\overline{u_i' u_j'} = \mu_t\left(\frac{\partial u_i}{\partial x_j} + \frac{\partial u_j}{\partial x_i}\right) \tag{4}$$

The turbulent viscosity term μ_t is to be computed from an appropriate turbulence model. The expression of the turbulent viscosity is given as [20]:

$$\mu_t = \rho C_\mu \frac{k^2}{\varepsilon} \tag{5}$$

where k, named as turbulence kinetic energy (TKE), is obtained from the following equation [20]:

$$\frac{\partial}{\partial x_i}\left[\rho k u_i\right] = \frac{\partial}{\partial x_j}\left[\left(\mu + \frac{\mu_t}{\sigma_k}\right)\frac{\partial k}{\partial x_j}\right] + G_k - \rho\varepsilon \tag{6}$$

Similarly, in the dissipation rate of TKE, ε, is presented by the following equation [20]:

$$\frac{\partial}{\partial x_i}\left[\rho\varepsilon u_i\right] = \frac{\partial}{\partial x_j}\left[\left(\mu + \frac{\mu_t}{\sigma_\varepsilon}\right)\frac{\partial \varepsilon}{\partial x_j}\right] + C_{1\varepsilon}\frac{\varepsilon}{k}G_k + C_{1\varepsilon}\rho\frac{\varepsilon^2}{k} \tag{7}$$

where G_k is the rate of generation of the TKE while $\rho\varepsilon$ is its destruction rate. G_k is written as [20]:

$$G_k = -\rho\overline{u_i' u_j'}\frac{\partial u_j}{\partial x_i} \tag{8}$$

The boundary values for the turbulent quantities near the wall are specified with the enhanced wall treatment method. C_μ=0.09, $C_{1\varepsilon}$=1.44, $C_{2\varepsilon}$=1.92, σ_k=1.00, σ_ε=1.30 and Pr_t=0.90 are chosen as empirical constants in the turbulence transport equations [20].

The fluid is considered to be Newtonian, and the physical properties of the fluid are temperature dependent. Since the temperature variation is higher than 3°C [21], the following polynomial expressions are used [22]:

$$\rho(T) = 5.3738\cdot10^{-10}T^5 - 9.59976\cdot10^{-7}T^4 + 6.93809\cdot10^{-4}T^3 - 0.255822T^2 + 47.8074T - 2584.53 \tag{9}$$

$$c_p(T) = -4.51782\cdot10^{-8}T^5 + 7.61613\cdot10^{-5}T^4 - 5.12699\cdot10^{-2}T^3 + 17.2363T^2 - 2894.85T + 198532 \tag{10}$$

$$k(T) = 5.15307\cdot10^{-11}T^5 - 8.15212\cdot10^{-8}T^4 + 5.138\cdot10^{-5}T^3 - 1.61344\cdot10^{-2}T^2 + 2.52691T - 157.532 \tag{11}$$

$$\mu(T) = -4.37087\cdot10^{-13}T^5 + 7.38482\cdot10^{-10}T^4 - 4.99292\cdot10^{-7}T^3 + 1.68946\cdot10^{-4}T^2 - 2.86313\cdot10^{-2}T + 1.94641 \tag{12}$$

To close the system of governing equations, a set of boundary condition is required. Velocity inlet for inlet, pressure outlet for outlet and non-slip with zero heat transfer between the fluid and side for side and a lower surface, non-slip with constant heat transfer for the upper surface of collector were applied as follows.

$$\begin{aligned}&\text{inlet:} && u = u_{in}, && v = 0, && T = T_{in}\\ &\text{outlet: } p = p_0\\ &\text{Side and lower surface:} && u = v = 0, && \partial T/\partial n = 0\\ &\text{Upper surface:} && u = v = 0, && q_{in} = -k\,\partial T/\partial y\end{aligned} \tag{13}$$

The spectral radiative transfer equation (RTE) can be written as [23]:

$$\frac{dI_v(r,s)}{ds} = -(K_{av} + K_{sv})I_v(r,s) + K_{av} I_b(v,T) + \frac{K_{sv}}{4\pi}\int_{4\pi} dI_v(r,s')\cdot\phi(s.s')d\Omega' + S \quad (14\text{-a})$$

where I_v is spectral radiation intensity which depends on position r and direction s [23]:

$$I_v(r,s) = \varepsilon_v(r_w)I_b(v,T) + \frac{\rho_w(r_w)}{\pi}\int_{n\cdot s'<0} I_v(r,s')\cdot|n.s'|d\Omega' \quad (14\text{-b})$$

The commercially available CFD software, FLUENT 15.0 was used to solve the governing equations. The control volume approach was used to solve the system of classical single phase governing equations by using the finite volume method (FVM). The standard k–ε turbulence model with the enhanced wall function was selected. The diffusion term in the momentum and energy equations was approximated by the second-order central difference. In addition, a second-order upwind differencing scheme was adopted for the convective terms. The convergence criterion was considered 10^{-6} for all variables.

2- 3- Energy modelling

Useful received energy by fluid in the collector is calculated as follows [24]:

$$\dot{Q}_{u,f} = \dot{m}_f c_p (T_{out} - T_{in}) \quad (15)$$

where $\dot{m}_f$ is the working fluid mass flow rate of, c_p is fluid constant specific heat capacity and T_{in} and T_{out} are the mean fluid inlet and outlet temperature, respectively.
Useful received energy by a collector based on inlet solar radiation and overall heat loss is as follows [24]:

$$\dot{Q}_{u,c} = A_c\left(S - U_L\left(T_{pm} - T_a\right)\right) \quad (16)$$

where A_c is the area of absorber plate, T_a is ambient temperature and T_{pm} is mean temperature of absorber plate. It should be noticed that the absorber plate temperature is not a constant value and considering its mean temperature, it is a virtual concept. In the present study, temperature gradients around the heat sink can be neglected and a mean temperature can be taken into account for it as far as heat sink has been spread through the absorber plate, and also the thermal conductivity of welding between plate and sink, thermal conductivity of plate and the convection heat transfer coefficient of fluid are high. Also in Eq. (16), S is a part of solar radiation per plate area unit that is absorbed by the plate and is as follows [24]:

$$S = \eta_0 \cdot I_T \quad (17)$$

where I_T is daily average hourly radiation entered to the collector and η_0 is an optical efficiency of collector and is calculated as follows [24]:

$$\eta_0 = (\tau\alpha) = 1.01\tau\cdot\alpha \quad (18)$$

where τ and α refer to solar transmission and solar absorption coefficient. Also, I_T is calculated as follows [24]:

$$I_T = I_b R_b + I_d\left(\frac{1+\cos\beta}{2}\right) + I\cdot\rho_{gr}\left(\frac{1-\cos\beta}{2}\right) \quad (19)$$

where I, I_b and I_d are solar radiation on the horizontal surface, beam radiation and diffuse radiation, respectively.
Also, R_b is the ratio of beam radiation on the tilted surface to that on a horizontal surface and is calculated as follows [24]:

$$R_b = \frac{\cos(\varphi-\beta)\cos\delta\cos(\omega) + \sin(\varphi-\beta)\sin\delta}{\cos\varphi\cos\delta\cos\omega + \sin\varphi\sin\delta} \quad (20)$$

where φ is the latitude of collector location, δ is declination angle and ω is the hour angle.
Furthermore, U_L in Eq. (16) is collector overall heat loss coefficient and is calculated as follows [24]:

$$U_L = U_t + U_b + U_e \quad (21)$$

where U_t is top loss coefficient, U_b is back loss coefficient and U_e is edge loss coefficient. The top loss coefficient is calculated by Eqs. (22) to (26) [24]:

$$U_t = \left(\frac{N}{\frac{C}{T_{pm}}\left[\frac{T_{pm}-T_a}{N+f}\right]^e} + \frac{1}{h_w}\right)^{-1} + \frac{\sigma\left(T_{pm}+T_a\right)\left(T_{pm}^2+T_a^2\right)}{\frac{1}{\varepsilon_P+0.0059N\cdot h_w} + \frac{2N+f-1+0.133\varepsilon_P}{\varepsilon_g} - N} \quad (22)$$

$$f = \left(1+0.089h_w - 0.1166h_w\varepsilon_p\right)\left(1+0.07866N\right) \quad (23)$$

$$C = 520\left(1-0.000051\beta^2\right) \quad (24)$$

$$e = 0.430\left(1-\frac{100}{T_{pm}}\right) \quad (25)$$

$$h_w = 2.8 + 3V_w \quad (26)$$

where N is the number of glass covers, hw is wind heat transfer coefficient, V_w is wind velocity and σ is Stefan Boltzmann constant.
Fig. 2 shows the equivalent thermal network for the flat-plate

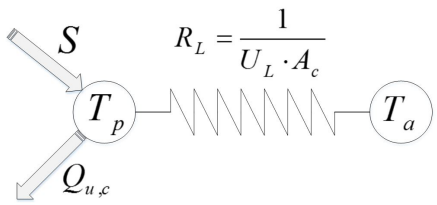

Fig. 2. Equivalent thermal network for solar collector

solar collector.
Also, the back loss coefficient is defined as follows [24]:

$$U_b = \frac{k}{L} \tag{27}$$

Energy efficiency of the collector is defined as follows [24]:

$$\eta = \frac{\dot{m}_f c_p \left(T_{out} - T_{in}\right) - \mathrm{P}_{pump}}{I_T A_c + \mathrm{P}_{agitator}} \tag{28}$$

where $P_{agitator}$ is the power of agitator and in maximum value is about 15 W per every cylindrical obstacle [25]. Also, P_{pump} is the power of pump and is defined as follows:

$$\mathrm{P}_{pump} = \frac{P_{flow}}{\eta_{pump}\eta_{motor}} \tag{29}$$

where η_{pump} and η_{motor} are the efficiency of pump and motor, respectively. Also, P_{flow} is the dynamic pressure drop of fluid and is calculated as follows:

$$P_{flow} = \frac{\dot{m}_f \Delta P}{\rho} \tag{30}$$

2- 4- Exergy modeling

Exergy is the available energy that is used. The rate of exergy equation is defined as follows [26]:

$$\dot{E}_{in} - \dot{E}_{out} - \dot{E}_{loss} - \dot{E}_{des} = \dot{E}_S \tag{31}$$

where $\dot{E}_S$ is the rate of storage exergy and it is equal to zero based on the assumption that the collector operates steady state condition. Also, $\dot{E}_{in}$ is the rate of inlet exergy, including rate of inlet exergy by inlet fluid to the collector ($\dot{E}_{in,f}$) and rate of inlet exergy of absorbed solar radiation ($\dot{E}_{in,Q}$).
The rate of inlet exergy by inlet fluid to the collector is defined as follows [26]:

$$\dot{E}_{in,f} = \dot{m} c_p \left(T_{in} - T_a - T_a \ln\left(\frac{T_{in}}{T_a}\right)\right) + \frac{\dot{m}\Delta P_{in}}{\rho} \tag{32}$$

where ΔP_{in} is the pressure difference between inlet fluid and ambient. The rate of inlet exergy of the absorbed solar radiation is defined as follows [26]:

$$\dot{E}_{in,Q} = \eta_0 I_T A_c \left(1 - \frac{T_a}{T_s}\right) \tag{33}$$

The temperature of the sun is about 5777 K based on the assumption that the sun is a black–body. Considering the influence of atmosphere on debilitation of solar radiation, T_s that is called the seeming temperature of the sun is about 0.75 of sun temperature and is equal to 4333 K, approximately [27].
Ėout is the rate of outlet exergy and includes the rate of outlet exergy by exiting fluid of collector ($\dot{E}_{out,f}$) [28].

$$\dot{E}_{out,f} = \dot{m} c_p \left(T_{out} - T_a \ln\left(\frac{T_{out}}{T_a}\right)\right) + \frac{\dot{m}\Delta P_{out}}{\rho} \tag{34}$$

where ΔP_{out} is the difference between the pressure of outlet fluid and ambient. Ėloss is the rate of exhausted exergy and includes the rate of exhausted exergy from plate to ambient ($\dot{E}_{l,p}$) and exhausted optical exergy ($\dot{E}_{L,optical}$).
The rate of exhausted exergy from plate to ambient is defined as follows [29]:

$$\dot{E}_{l,p} = U_L A_c \left(T_{pm} - T_a\right)\left(1 - \frac{T_a}{T_{pm}}\right) \tag{35}$$

Due to optical properties of the plate, a part of the solar radiation is not absorbed. Collector exhausted optical exergy is calculated as follows [30]:

$$\dot{E}_{L,optical} = \frac{\left(1-\eta_0\right)\dot{E}_{in,r}}{\dot{E}_{in,r}} = 1 - \eta_0 \tag{36}$$

$\dot{E}_{des}$ is the rate of destroyed exergy due to temperature gradients between plate and sun ($\dot{E}_{d,\Delta Tp\text{-}s}$), temperature gradients between plate and fluid ($\dot{E}_{d,\Delta Tf}$) and pressure drop from inlet to outlet caused by viscosity of fluid, effects of walls of heat sink and also obstacles ($\dot{E}_{d,\Delta P}$). These parameters are calculated as follows, respectively [26]:

$$\dot{E}_{d,\Delta T_{p-s}} = \eta_0 I_T A_c T_a \left(\frac{1}{T_p} - \frac{1}{T_s}\right) \tag{37}$$

$$\dot{E}_{d,\Delta T_f} = \dot{m} c_p T_a \ln\left(\frac{T_{out}}{T_{in}}\right) - \dot{m} c_p T_a \frac{T_{out} - T_{in}}{T_p} \tag{38}$$

$$\dot{E}_{d,\Delta p} = \frac{\dot{m}\Delta p T_a \ln\left(\frac{T_{out}}{T_{in}}\right)}{\rho\left(T_{out} - T_{in}\right)} \tag{39}$$

Exergy efficiency of flat–plate solar collector is defined as the rate of exergy increasing fluid in the collector to the exergy of entering solar radiation to the collector and is calculated as follows [17]:

$$\psi = \frac{\dot{E}_{out,f} - \dot{E}_{in,f}}{I_T A_C \left(1 - \frac{T_a}{T_s}\right) + \mathrm{P}_{agitator}} \tag{40}$$

By combining Eqs. (27) and (36), the exergy efficiency of water-based flat–plate solar collector equipped with

stationary and rotational obstacles is achieved.

2- 5- Validation

A non-uniform grid has been used in this study and Fig. 3 shows a grid layout near obstacles. As can be seen, a triangular mesh was obtained. The triangular mesh can present a better response in the view of precision. A grid independence test was performed for the collector with three rotational obstacles having a rotational velocity of 2 rad/s at 12 p.m. to analyze the effects of grid sizes on the results.

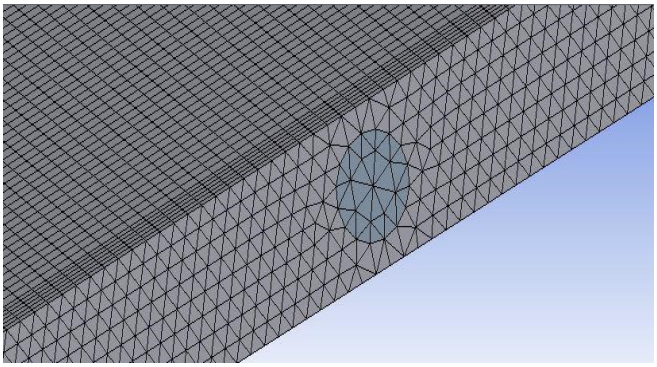

Fig. 3. Grid layout used in the present work

As shown in Table 3, seven sets of meshes are generated and tested. By comparing the results, it is concluded that mesh configurations contain grid number of 3,728,623 nodes adopted to get an acceptable compromise between the computational time and the result accuracy.

Table 3. Grid independence test

Nodes	T_{out},°C	Error (%)
421,761	41.8481	23.64
1,818,109	51.7307	16.20
2,701,751	61.1101	9.10
3,243,983	66.6782	2.22
3,599,007	70.5134	1.05
3,728,623	70.7811	0.02
3,954,131	70.7834	-

The computer software validation by comparison of numerical results was obtained from the present study and empirical data of Khorasanizadeh et al. [5] at the same geometrical dimension and boundary condition, (Fig. 4). As can be seen from Fig. 4 a very good agreement between the empirical data [5] and numerical results obtained from the present study exists.

It is worth noting that the difference between empirical and numerical data is low in all hours except three points. One can relate this phenomenon to inaccuracy that (probably) exists in empirical data.

3- Results and Discussion

In this section, at first the collector exergy analysis is presented in three different conditions and then the optimization case is investigated.

Fig. 5 presents the temperature contour around an obstacle for (a) stationary and (b) rotational cases. As can be seen,

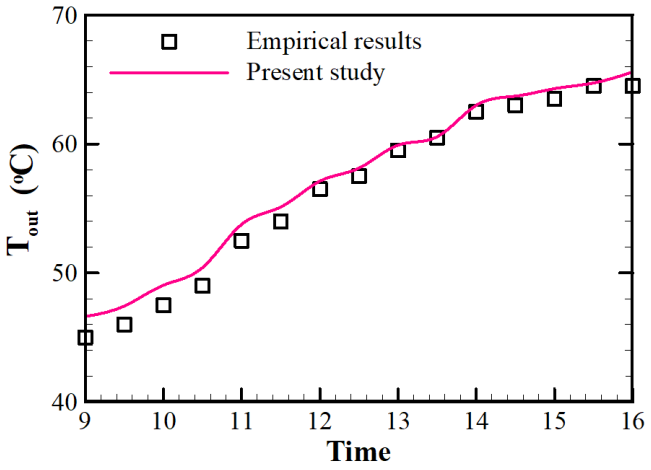

Fig. 4. Comparison of the present results with the empirical results of Khorasanizadeh et al. [5], in terms of outlet fluid temperature

by using from obstacle, a significant effect on temperature distribution can be distinguished.

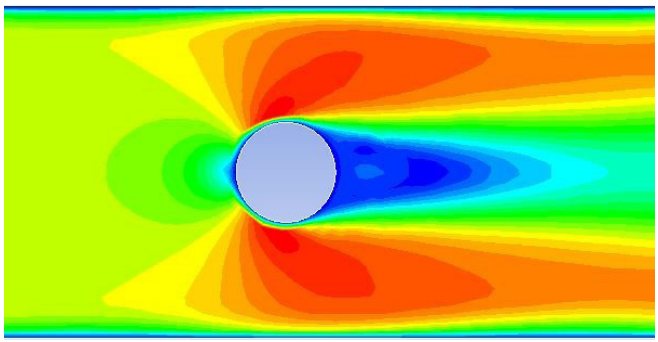

(a)

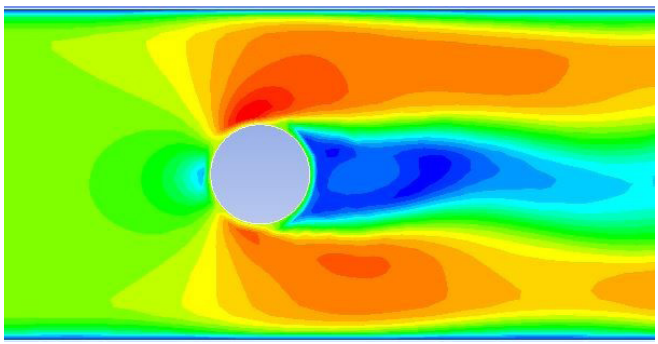

(b)

Fig. 5. Temperature contour for (a) stationary and (b) rotational obstacle.

3- 1- Energy and exergy efficiencies

The total heat loss coefficient, mean temperature of absorber plate, collector outlet temperature and energy and exergy efficiencies of the simple heat sink (SHS) collector, heat sink collector equipped with stationary obstacles (HSSO) and heat sink collector equipped with rotational obstacles (HSRO) in different hours of a day are reported in Tables 4 to 6, respectively. All these values are obtained based on

numerical results and analytical correlation.

It is realized that energy and exergy efficiencies of SHS collector increase by 30% and 60%, respectively, compared with the reference collector [5] owing to the more wetted surface between plate and fluid and more time that takes the fluid pass the route. Also, the energy efficiency of HSSO and HSRO increases by about 39% and 48%, respectively, in comparison to the reference collector because of the induction of high disturbance and thin boundary layer in the channels equipped with obstacles, leading to a higher temperature gradient from the inlet to outlet.

On the other side, the exergy efficiency of HSSO and HSRO increases by about 116% and 120%, respectively, compared with the reference collector.

Furthermore, the mean temperature of the plate and outlet temperature of the collector increase during the day incessantly because of the collector inlet temperature of the fluid that is taken from the reservoir, which constantly increase due to the collector performance in a closed loop and heat saving in the reservoir. Also, in all conditions the inlet radiation flux rate increases from morning to the middle day hours and then decreases. The energy efficiency has the same trend.

Table 4. Results of simple heat sink collector (SHS)

Time	U_L W/m²·K	T_{pm} ,°C	T_{out} ,°C	η , %	ψ , %
09:00	7.33	48.11	58.59	54.29	3.34
09:30	7.37	49.06	59.61	57.48	3.53
10:00	7.32	51.32	61.04	57.78	3.95
10:30	7.49	52.41	62.61	64.40	4.21
11:00	7.56	54.25	65.82	63.00	4.35
11:30	7.52	57.07	67.07	63.68	4.58
12:00	7.56	58.42	69.23	61.91	4.60
12:30	7.77	59.31	70.26	61.54	4.55
13:00	7.76	60.46	72.04	61.48	4.54
13:30	7.40	60.57	72.61	60.16	4.68
14:00	7.73	63.22	75.13	58.64	4.67
14:30	7.55	63.47	75.77	57.57	4.56
15:00	7.77	63.89	76.41	56.91	4.41
15:30	7.94	64.09	76.91	56.28	4.21
16:00	7.97	65.11	77.82	55.62	4.15

However, the reason for decreasing the energy efficiency after the afternoon hours increases the inlet fluid temperature and also increases the absorber plate temperature as time passes that intensifies the losses.

It is clear from Tables 4 to 6 that the U_L change in different hours is significant so that in the condition of the collector with simple heat sink the relative difference of U_L at 10 a.m. is about 9% compared to 16 p.m. This difference is more for other cases. This fact shows that the assumption of constant U_L that some researchers have considered is not logical and it is necessary to apply its changes in measurements.

3- 2- Analyze and exergetic optimization

For all three conditions of using the collector, the lowest exergy, and energy analysis is related to 9 a.m. either energy efficiency or exergy efficiency that are dependent on the I_T and radiation angle. At 9 a.m. the IT is less and also the angle between the direct horizontal sun radiation and vertical to the collector surface is high. Hence the sun radiation absorption is less. In addition, the collector performance due to the change in I_T, radiation angle and also the change in temperature of collector water inlet is always transient. These conditions are of high importance in the beginning hours of the day and these are factors of decreasing the efficiency. The effect of changing T_a, I_T, T_{in}, η_0 and $\dot{m}$ on exergy efficiency for the three conditions at this time was studied to optimize the collector exergically. Therefore, when different values were considered

Table 5. Results of the simple heat sink collector (HSSO)

Time	U_L W/m²·K	T_{pm} ,°C	T_{out} ,°C	η , %	ψ , %
09:00	7.13	47.85	61.67	65.39	3.81
09:30	7.21	48.35	62.76	69.79	4.01
10:00	7.24	50.87	64.34	70.28	4.48
10:30	7.26	51.88	65.91	74.51	4.80
11:00	7.37	54.81	68.77	77.57	4.96
11:30	7.44	57.36	69.67	78.51	5.22
12:00	7.48	58.76	72.45	76.00	5.29
12:30	7.56	59.45	73.92	77.54	5.23
13:00	7.61	60.36	75.63	81.48	5.27
13:30	7.04	61.57	76.71	83.62	5.42
14:00	7.51	62.67	78.38	79.50	5.41
14:30	7.39	62.82	78.78	75.00	5.28
15:00	7.30	63.48	79.65	74.11	5.11
15:30	7.42	64.88	79.71	71.21	4.88
16:00	7.45	64.87	79.79	67.31	4.81

Table 6. Results of simple heat sink collector (HSRO)

Time	U_L W/m²·K	T_{pm} ,°C	T_{out} ,°C	η , %	ψ , %
09:00	6.78	47.56	62.44	78.22	3.92
09:30	6.83	48.47	63.66	79.64	4.11
10:00	6.88	50.56	64.96	80.48	4.62
10:30	6.92	51.74	66.77	89.61	4.92
11:00	6.96	54.14	68.91	87.24	5.05
11:30	6.93	57.74	70.46	88.14	5.34
12:00	6.95	58.25	73.85	86.23	5.45
12:30	6.97	59.63	74.96	61.53	5.46
13:00	6.98	60.16	76.57	85.41	5.37
13:30	6.97	61.80	77.85	83.44	5.51
14:00	6.84	62.11	78.98	82.51	5.56
14:30	6.79	62.27	79.74	85.22	5.41
15:00	6.75	63.83	80.36	79.11	5.21
15:30	6.71	64.56	80.24	78.21	4.98
16:00	6.74	64.92	80.11	77.21	4.85

for one parameter, the values at 9 a.m. were assigned to other parameters. The results related to the influence of changing different parameters on the exergy analysis are shown in Figs. 6 to 10.

In Fig. 6, the exergy efficiency variation with sun radiation flux is presented. In the radiation flux changing period, from 300 to 1200 W/m^2, for three studied cases, an increasing trend for exergy efficiencies is observed.

By increasing the sun radiation flux, the temperature of collector fluid outlet increases and this increase leads to

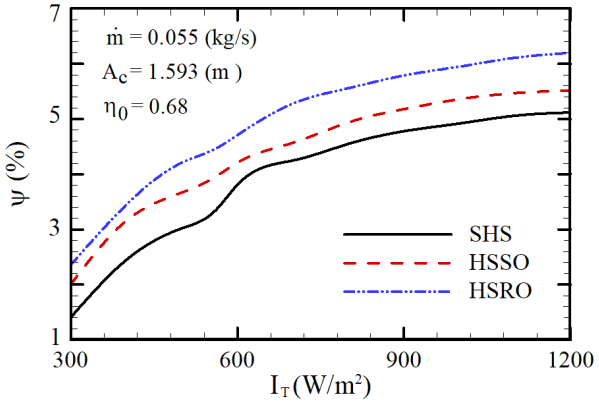

Fig. 6. Variation of exergy efficiency of a collector with solar radiation

exergy efficiency increment. In addition, a non–uniformity in the trend of exergy efficiency variation is seen for three studied cases. An important point in the referred phenomena is that this behavior is seen in three studied cases. Authors thought, at this point, a change in the regime of the fluid flow has occurred. In fact, a change in the flow regime can damage the boundary layers that leads to increasing efficiency and fluctuation of exergy efficiency.

Employing ribs, grooves or obstacles in the channels have been one of the frequent approaches to break the laminar sub-layer and create local turbulence due to flow separation and reattachment between successive corrugations, which reduces the thermal resistance and significantly enhances the heat transfer. On the other hand, the large Reynolds number is attributed to the higher velocity which can lead to disturbing the flow and thus, the heat transfer is strengthened [31–33]. In all cases of Fig. 6, the flows of sink equipped with obstacles gave higher values of turbulence than that for smooth sink flow. Since the presence of local turbulences can make some non–uniformity during heat transfer and pressure drop increasing,the non–uniformities during exergy increasing in Fig. 6 may be caused by turbulent regime effects.

The exergy efficiency variation with the collector inlet fluid temperature has been demonstrated in Fig. 7. For three studied cases, primarily the exergy efficiency increases until the temperature reaches about 65 to 70°C and then it has a decreasing trend. On the one hand by T_{in} increase, the outlet temperature increases that leads to exergy efficiency increment. On the other hand, Tin increases means the fluid temperature inside the collector increase which raises the thermal loss. Thus, there is one optimum T_{in} that for higher temperatures, the effect of exergy efficiency reduction due to a higher thermal loss is greater than its increase effect. The variation of exergy efficiency with an ambient temperature has been shown in Fig. 8.

For three studied cases, the exergy efficiency has a decreasing trend with an ambient temperature increase. In Fig. 8, the

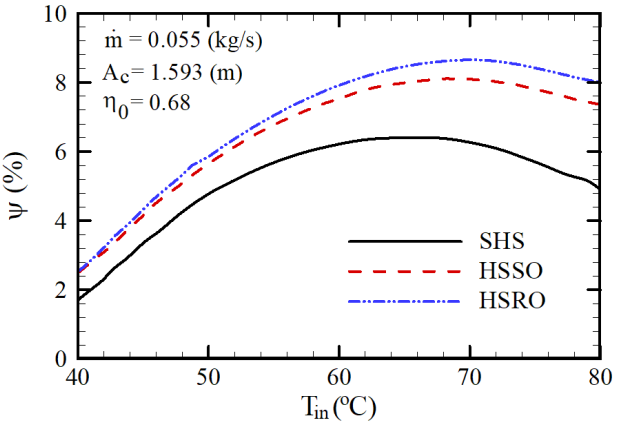

Fig. 7. Variation of exergy efficiency of a collector with ther temperature of the inlet fluid

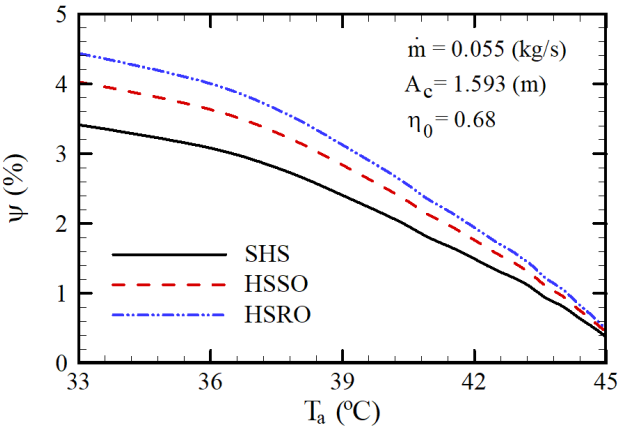

Fig. 8. Variation of exergy efficiency of a collector with the ambient temperature

effects of using obstacles in exergy efficiency increase due to the heat transfer rate between working fluid and collector.

In Fig. 9, the influence of increasing optical efficiency on exergy efficiency has been demonstrated.

By optical efficiency increment for three studied cases, the radiation absorption by the absorber plate enhances and leads to increasing the fluid temperature inside the collector and therefore the exergy efficiency increases.

In Fig. 10, the effect of changing the working fluid mass flow rate passing through the collector is shown in three studied cases, for mass flow rates from 0 to 0.1 kg/s. It is worth noting that the applied mass flow rate for three studied cases, in Tables 4 to 6, was about 0.055 kg/s. By referring to the results presented in Fig. 10, it must be noted that in the three studied cases, the used parameters such as ambient temperature, inlet fluid temperature, optical efficiency, radiation flux and collector cross-section have the same values mentioned in Tables 4 to 6 that are related to 9 a.m.

For the collector with the simple heat sink, i.e. without extra equipment, the optimum mass flow rate that causes the exergy efficiency to be maximum, should be ten times lower that the above value (0.055 kg/s), that means 0.005

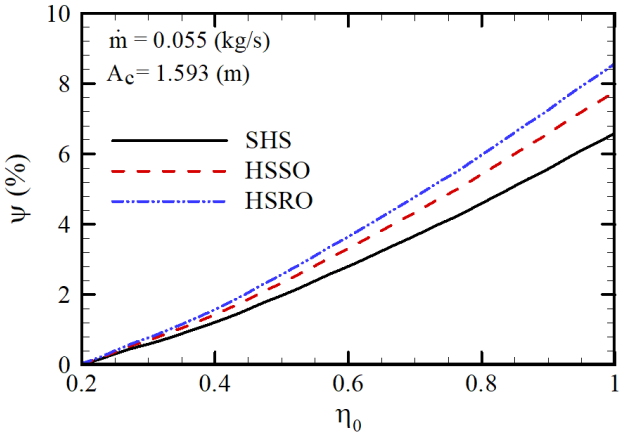

Fig. 9. Variation of exergy efficiency of a collector with an optical efficiency

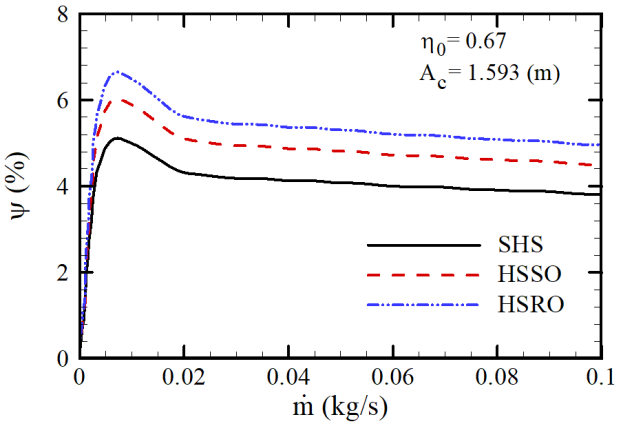

Fig. 10. Variation of exergy efficiency of the collector with the mass flow rate of fluid

kg/s. Consequently the exergy efficiency is 5.3% (for 0.005 kg/s), instead of being 4% (for 0.055 kg/s). Nevertheless, for the condition of using stationary and rotational obstacles the maximum exergy efficiency occurs in the optimum mass flow rate of 0.0075 kg/s. It is clear that in the case of using a simple heat sink (SHS, HSSO, and HSRO), the time when the fluid is inside the collector increases and causes outlet temperature to increase from the collector and the exergy efficiency increases. About the parameters that can influence the exergy efficiency with the mass flow rate, it must be said that increasing the mass flow rate increases the absorbing energy due to the lower fluid temperature. On the other hand, the need to additional pumping power decreases the exergy efficiency. One can obtain another parameter that can have negative or positive effects on exergy efficiency by varying mass flow rate. The flow rate of 0.055 kg/s is the mass flow rate at which the positive effect is equal to a negative effect and after which the negative effects are greater than positive effects. In addition to the above results, the values of outlet temperature for three studied cases with the mass flow rate was presented in Table 7. As can be seen, the outlet temperature in HSSO is higher than SHS collector and in HSRO is higher than HSSO collector. This phenomenon is due to the fact that the extra equipment exists in each collector. Although the difference between these values is low, its effect on efficiency is considerable.

Table 7. Variation of outlet temperature (°C) of the collector with the mass flow rate of fluid

Mass flow rate, kg/s	Model		
	SHS	HSSO	HSRO
0.01	57.00	57.39	57.88
0.02	57.09	57.45	58.32
0.03	57.53	58.00	58.68
0.04	58.09	59.21	60.24
0.05	58.54	61.62	62.41
0.06	59.67	60.01	60.56
0.07	61.88	62.13	62.58
0.08	63.90	64.55	65.01
0.09	64.95	66.07	66.20
0.10	66.13	67.02	67.56

3- 3- Rotational obstacle velocity and direction effect on outlet temperature and exergy efficiency of HSRO collector

The effect of velocity and direction of a rotational obstacle on outlet temperature and exergy efficiency of HSRO collector was investigated numerically.

The results of the refereed investigation were presented in Table 8. As the results show, the direction of rotational obstacle does not have any effect on outlet temperature and exergy efficiency. One can relate this phenomenon to the low obstacle rotational velocity that the direction of rotational obstacle does not have any effect on the results. On the other hand, the magnitude of obstacle velocity has a significant effect on outlet temperature and exergy efficiency.

Table 8. Obstacles rotational velocity and direction effect on the outlet temperature and exergy efficiency of HSRO collector

Model	Rotation Direction	V_o, rad/s	T_{out}, °C	ψ, %
HSRO.1	C.W.	1.00	61.68	3.37
HSRO.2	A.C.W.	1.00	61.69	3.37
HSRO.3	C.W.	2.00	62.44	3.92
HSRO.4	A.C.W.	2.00	62.46	3.92
HSRO.5	C.W.	3.00	63.67	3.75
HSRO.6	A.C.W.	3.00	63.71	3.75

It is worth noting that rotational velocity of 2 rad/s has a higher exergy efficiency than others. In addition, the velocity of rotational obstacle has two separate effects on the fluid flow and heat transfer. From one hand, mixing the fluid augments the friction and destroys the kinetic energy, from the other hand, mixing the fluid eliminates the thickness of the boundary layer and enhances the heat transfer. Comparison of the two referred effects is a factor that changes the exergy efficiency. In other words, utilizing rotational obstacles with higher velocities has a better heat transfer performance but also a more pressure drop penalty. Therefore the usage of rotational obstacles with 3 rad/s velocity has a lower exergy efficiency as compared with the model with 2 rad/s velocity. As can be seen from the obtained results by increasing the obstacle rotational velocity, the negative effect overcomes the

positive effect and rotational velocity equal to 2 rad/s was the optimum point in the viewpoint of exergy efficiency.

4- Conclusions

Specifying some values of mass flow rate and other parameters that the exergy efficiency gets maximum due to them is difficult but in the concept of exergy efficiency, the effect of these parameters is clearer. In this study, the optimization of a solar collector was done in a closed circuit for three conditions in the viewpoint of exergy analysis by assuming that U_L is the only variable parameter and the fluid temperature is not equal to ambient temperature. The effect of using the stationary and rotational obstacles through fluid passage was studied and these results were obtained:

- The increase in solar radiation flux and optical efficiency leads to exergy efficiency increase for all conditions.
- The exergy efficiency decreases with ambient temperature increase, but by increasing the collector inlet fluid temperature, the exergy efficiency increases to the certain temperature and then decreases.
- For each special collector, there is a unique mass flow rate that the exergy efficiency gets maximum (0.005 kg/s). For higher mass flow rates, primarily the exergy efficiency slightly decreases and then remains unchanged.
- Generally, using the stationary and rotational obstacles enhances the exergy efficiency. Nevertheless, using the rotational obstacles is more suitable than using the stationary obstacles. Generally, while the trend of exergy efficiency variation with effective parameters is increasing, applying the obstacles precipitates the exergy efficiency increment efficiency (from 4% to 5.3%). In addition, for the case that the trend of exergy efficiency variation by changing these parameters is decreasing, the decreasing trend gets slow.
- For the analyzed collector in this study for all three conditions of using the simple heat sink, stationary and rotational obstacles, the increase in fluid inlet temperature and optical efficiency leads to more increase in exergy efficiency.
- The collector performance in a closed circuit causes the collector inlet fluid temperature to increase constantly in the condition that the reservoir temperature increases due to not using the stored heat in it. The temperature increase leads to exergy efficiency increase to a certain point and then decreases this efficiency for the higher values.

References

[1] S. A. Kalogirou, Solar thermal collectors and applications. *Progress in Energy and Combustion Science*, 30(3) (2004) 31-95.

[2] M. Ansari, M. Bazargan, Optimization of Heat transfer and Pressure Drop in a Solar Air Heater with Ribbed Surface. *Amirkabir Journal of Mechanical Engineering*, 49(1) (2017) 137-146.

[3] Z. Poolaei Moziraji, A. Azimi, S. Kazemzadeh Hannani, M. Najafi, Simultaneous Estimation of Thermophysical Properties and Convective Boundary Conditions of a Sample Room in Tehran Using Inverse Analysis. *Amirkabir Journal of Mechanical Engineering*, 49(1) (2017) 147-160.

[4] H. Jahani, A. Abbassi, M. Kalteh, M. Azimifar, Semi-Analytic Solution of Nanofluid and Magnetic Field Effects on Heat Transfer from a Porous Wall. *Amirkabir Journal of Mechanical Engineering*, 49(1) (2017) 161-170.

[5] H. Khorasanizadeh, A. Aghaei, H. Ehteram, A. Azimi, Study and Exergy Optimization of a Flat Plate Solar Collector in a Closed Circuit Utilized with Reflectors and Lenses Using Experimental Results. *Journal of Energy Engineering Management*, 3(1) (2013) 40-51.

[6] M. A. Leon, S. Kumar, Mathematical modeling and thermal performance analysis of unglazed transpired solar collectors. *Solar Energy*, 81 (2007) 62-75.

[7] S. Motahar, A. A. Alemrajabi, An analysis of unglazed transpired solar collectors based on exergetic performance criteria. *International Journal of Thermodynamics*, 13(4) (2010) 153-160.

[8] C. F. Kutscher, C. B. Christensen, G. M. Barker, Unglazed transpired solar collectors: heat loss theory. *Journal of Solar Energy Engineering*, 115 (1993) 182-188.

[9] C. Yildiz, I. T. Torgrul, C. Sarsilmaz, D. Pehlivan, Thermal efficiency of an air solar collector with extended absorption surface and increased convection. *International Communication in Heat and Mass Transfer*, 29(6) (2002) 831-840.

[10] P. T. Tsilingiris, Heat transfer analysis of low thermal conductivity solar energy absorbers. *Applied Thermal Engineering*, 20 (2000) 1297-1314.

[11] N. M. Khattab, Evaluation of perforated plate solar air heater. *International Journal of Solar Energy*, 21 (2000) 45-62.

[12] D. Njomo, M. Daguenet, Sensitivity analysis of thermal performances of flat plate solar air heaters. *Heat and Mass Transfer*, 42 (2006) 1065-1081.

[13] A. Sarreshtedari, A. Zamani Aghaee, Investigation of the thermo-hydraulic behavior of the fluid flow over a square ribbed channel. *Journal of Heat and Mass Transfer Research*, 1(2) (2014) 101-106.

[14] Z. Baniamerian, R. Mehdipour, F. Kargar, A numerical investigation on aerodynamic coefficients of solar troughs considering terrain effects and vortex shedding. *International Journal of Engineering* (*IJE*)*, Transactions C: Aspects*, 28(6) (2015) 940-948.

[15] B. M. Ziapour, F. Rahimi, Numerical study of natural convection heat transfer in a horizontal wavy absorber solar collector based on the second law analysis. *International Journal of Engineering* (*IJE*)*, Transactions A: Basics*, 29(1) (2016) 109-117.

[16] K. Ajay, L. Kundan, Performance evaluation of nanofluid (Al2O3/H2O–C2H6O2) based parabolic solar collector using both experimental and CFD techniques. *International Journal of Engineering* (*IJE*)*, Transactions A: Basics*, 29(4) (2016) 572-580.

[17] I. Luminosu, L. Fara, Determination of the optimal operation mode of a flat solar collector by exergetic analysis and numerical simulation. *Energy*, 30(12) (2005) 731-747.

[18] E. Shojaeizadeh, F. Veysi, Development of a correlation for parameter controlling using exergy efficiency

optimization of an Al2O3/water nanofluid based flat-plate solar collector. *Applied Thermal Engineering*, 98 (2016) 1116-1129.

[19] Z. Said, R. Saidur, N. A. Rahim, Energy and exergy analysis of a flat plate solar collector using different sizes of aluminum oxide based nanofluid. *Journal of Cleaner Production*, 133 (2016) 518-530.

[20] S. M. Vanaki, H. A. Mohammed, A. Abdollahi, M. A. Wahid, Effect of nanoparticle shapes on the heat transfer enhancement in a wavy channel with different phase shifts. *Journal of Molecular Liquids*, 196 (2014) 32-42.

[21] D. D. Gray, A. Giorgini, The validity of the Boussinesq approximation for liquids and gases. *International Journal of Heat and Mass Transfer*, 19(5) (1976) 545-551.

[22] A. Bejan, *Convection heat transfer*. Wiley-Interscience (1984).

[23] ANSYS Fluent-Solver Theory Guide, Release 14.0 (2011) 351-353.

[24] J. A. Duffie, W. A. Beckman, *Solar engineering of thermal processes*. New York, John Wiley & Son (2006).

[25] Mechanical Agitator Power Requirements for Liquid, www.pdhonline.com/courses/k103/k103content.pdf

[26] A. Suzuki, General theory of exergy balance analysis and application to solar collectors. *Energy*, 13(2) (1988) 123-160.

[27] A. Bejan, D. W. Keary, F. Kreith, Second law analysis and synthesis of solar collector systems. *Journal of Solar Energy Engineering*, 103(1) (1981) 23-28.

[28] A. Bejan, 1Advanced Engineering Thermo-dynamics. New York, Wiley Inter science (1988).

[29] K. K. Dutta Gupta, S. Saha, Energy analysis of solar thermal collectors. *Renewable energy and environment*, 33(1) (1990) 283-287.

[30] A. Kahrobaian, H. Malekmohammadi, Exergy optimization applied to linear parabolic solar collectors. *Journal of Faculty of Engineering*, 42(1) (2008) 131-144.

[31] A. A. Abbasian Arani, S. Sadripour, S. Kermani, Nanoparticle shape effects on thermal-hydraulic performance of boehmite alumina nanofluids in a sinusoidal–wavy mini-channel with phase shift and variable wavelength. *International Journal of Mechanical Sciences*, 128–129 (2017) 550-563.

[32] S. Sadripour, M. Adibi, G. A. Sheikhzadeh, Two Different Viewpoints about using Aerosol-Carbon Nanofluid in Corrugated Solar Collectors: Thermal-Hydraulic Performance and Heating Performance, *Global Journal of Researches in Engineering A: Mechanical and Mechanics*, 17(5) (2017) 19-36.

[33] H. Khorasanizadeh, S. Sadripour, A. Aghaei, Numerical Investigation of Thermo-Hydraulic Characteristics of Corrugated Air-Heater Solar Collectors, *Modares Mechanical Engineering*, 16(13) (2016) 42-46.

Please cite this article using:

S. Sadripour, A. A. Abbasian Arani, S. Kermani, Energy and Exergy Analysis and Optimization of a Heat Sink Collector Equipped with Rotational Obstacles, *AUT J. Mech. Eng.*, 2(1) (2018) 39-50.

DOI: 10.22060/mej.2017.12960.5486